**Supporting Information for**

**ORIGINAL ARTICLE**

# Structurally defined tandem-responsive nanoassemblies composed of dipeptide-based photosensitive derivatives and hypoxia-activated camptothecin prodrugs against primary and metastatic breast tumors

Mengchi Sun[a], Hailun Jiang[b], Tian Liu[a], Xiao Tan[a], Qikun Jiang[a], Bingjun Sun[b], Yulong Zheng[c], Gang Wang[d], Yang Wang[d], Maosheng Cheng[b], Zhonggui He[a,*], Jin Sun[a,*]

[a]*Wuya College of Innovation, Shenyang Pharmaceutical University, Shenyang 110016, China*

[b]*Key Laboratory of Structure-Based Drug Design and Discovery, Shenyang Pharmaceutical University, Ministry of Education, Shenyang 110016, China*

[c]*School of Materials Science and Engineering, Ocean University of China, Qingdao 266100, China*

[d]*College of Pharmacy, Guangxi University of Chinese Medicine, Nanning 530200, China*

Received 10 April 2021; received in revised form 10 May 2021; accepted 28 May 2021

*Corresponding authors. Tel./fax: +86 24 23986321 (Jin Sun); +86 24 23986321 (Zhonggui He).

E-mail addresses: sunjin@syphu.edu.cn (Jin Sun), hezhonggui@vip.163.com (Zhonggui He).

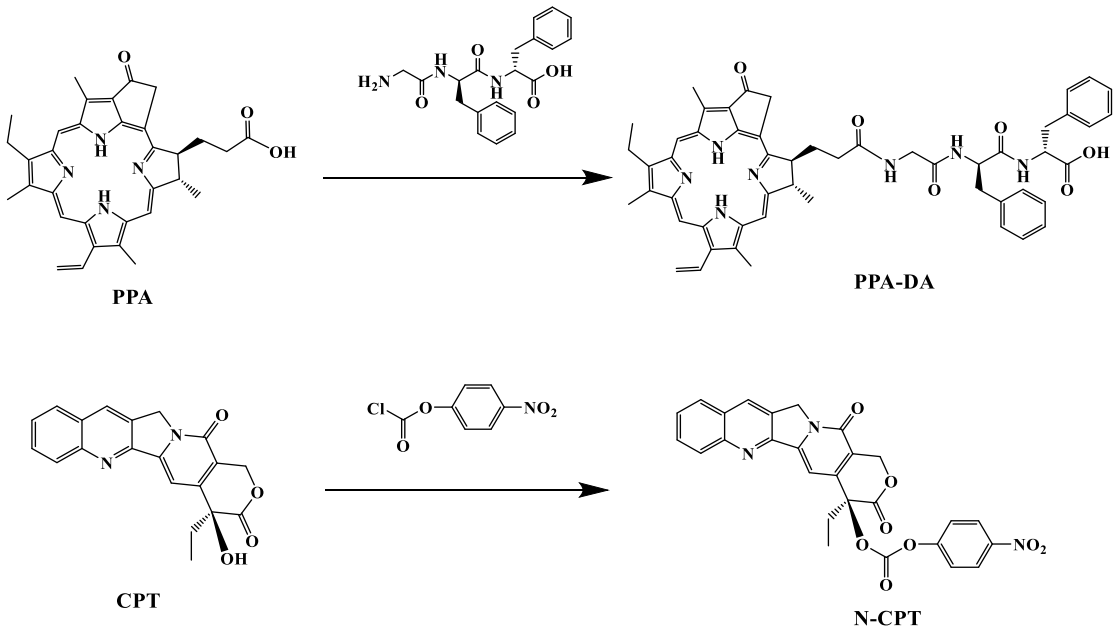


**Scheme S1** Synthetic route of the FF-based photosensitive prodrug (PPA-DA) and the hypoxia-activated camptothecin prodrug (N-CPT).

**A**

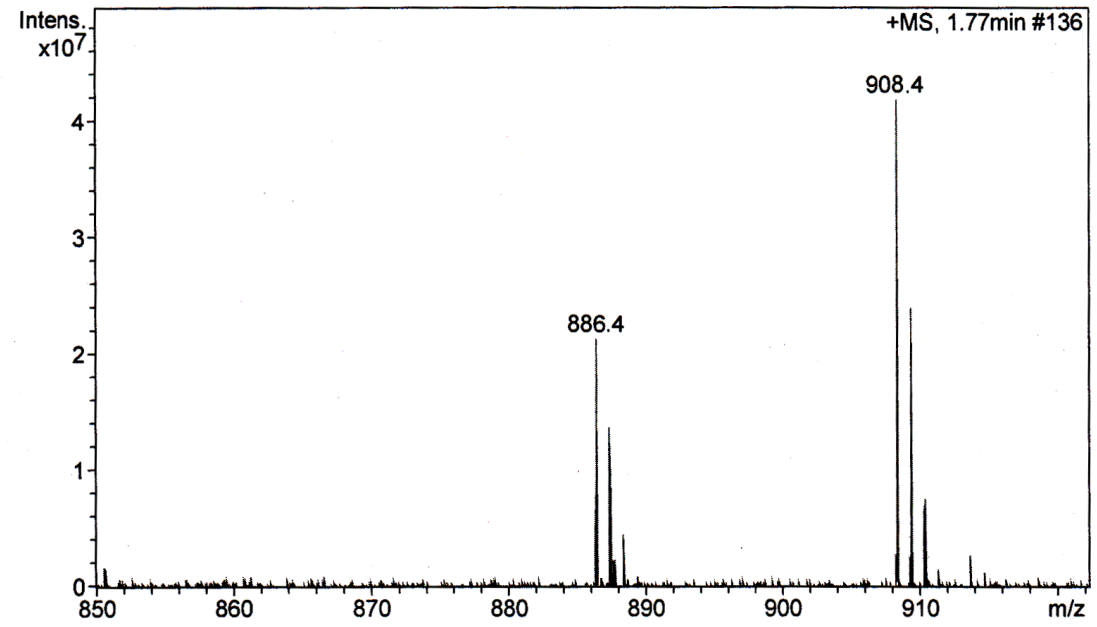


**B**

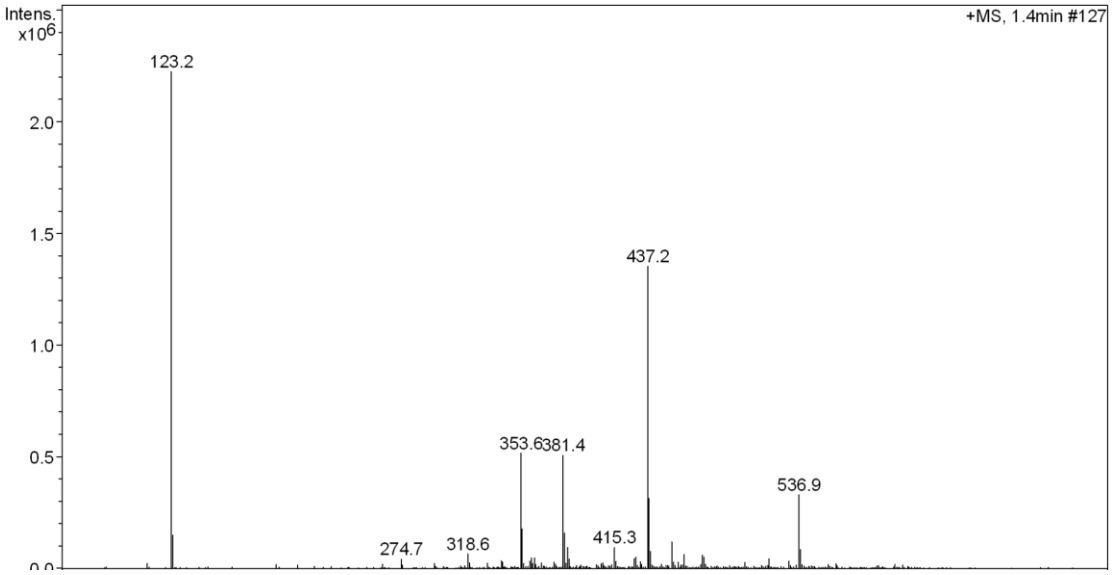


**Figure S1** Mass spectra of (A) the FF-based photosensitive prodrug (PPA-DA) and (B) the hypoxia-activated camptothecin prodrug (N-CPT).

**A**

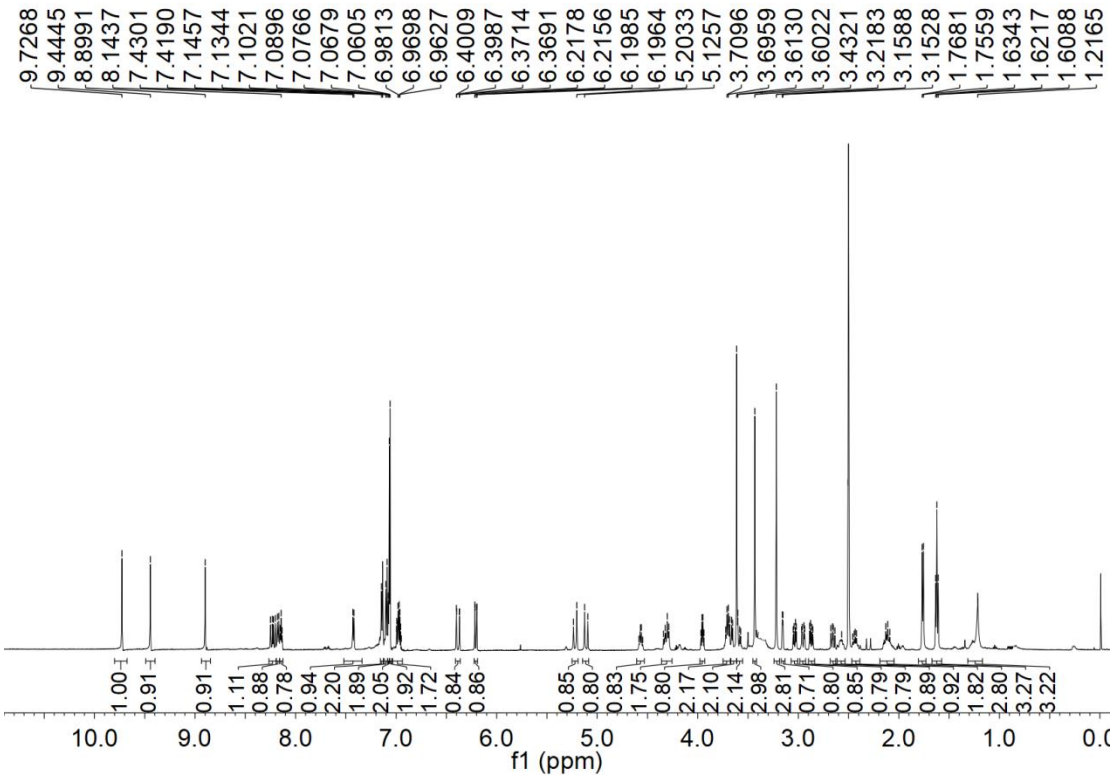
9.7268
9.4445
8.8991
8.1437
7.4301
7.4190
7.1457
7.1344
7.1021
7.0896
7.0766
7.0679
7.0605
6.9813
6.9698
6.9627
6.4009
6.3987
6.3714
6.3691
6.2178
6.2156
6.1985
6.1964
5.2033
5.1257
3.7096
3.6959
3.6130
3.6022
3.4321
3.2183
3.1588
3.1528
1.7681
1.7559
1.6343
1.6217
1.6088
1.2165
1.00
0.91
0.91
1.11
0.88
0.78
0.94
2.20
1.89
2.05
1.92
1.72
0.84
0.86
0.85
0.80
0.83
1.75
0.80
2.17
2.10
2.14
2.98
2.81
0.71
0.80
0.85
0.79
0.79
0.89
0.92
1.82
2.80
3.27
3.22
10.0
9.0
8.0
7.0
6.0
5.0
4.0
3.0
2.0
1.0
f1 (ppm)

**B**

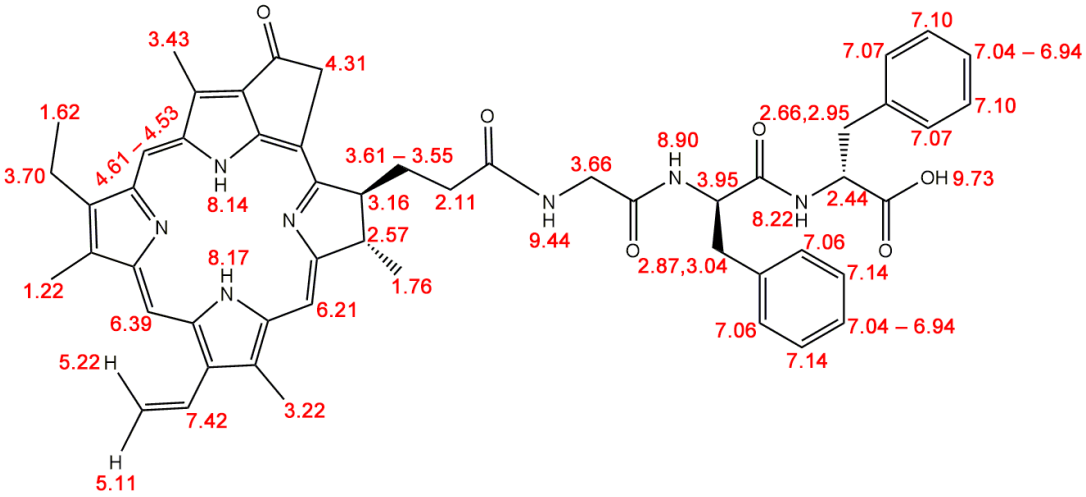
3.43
4.31
1.62
4.61 – 4.53
3.70
8.14
3.61 – 3.55
3.16
2.11
2.57
1.22
8.17
1.76
6.39
6.21
5.22
7.42
3.22
5.11
3.66
9.44
8.90
3.95
2.66,2.95
8.22
2.44
9.73
2.87,3.04
7.10
7.07
7.04 – 6.94
7.10
7.07
7.06
7.14
7.06
7.04 – 6.94
7.14

**C**

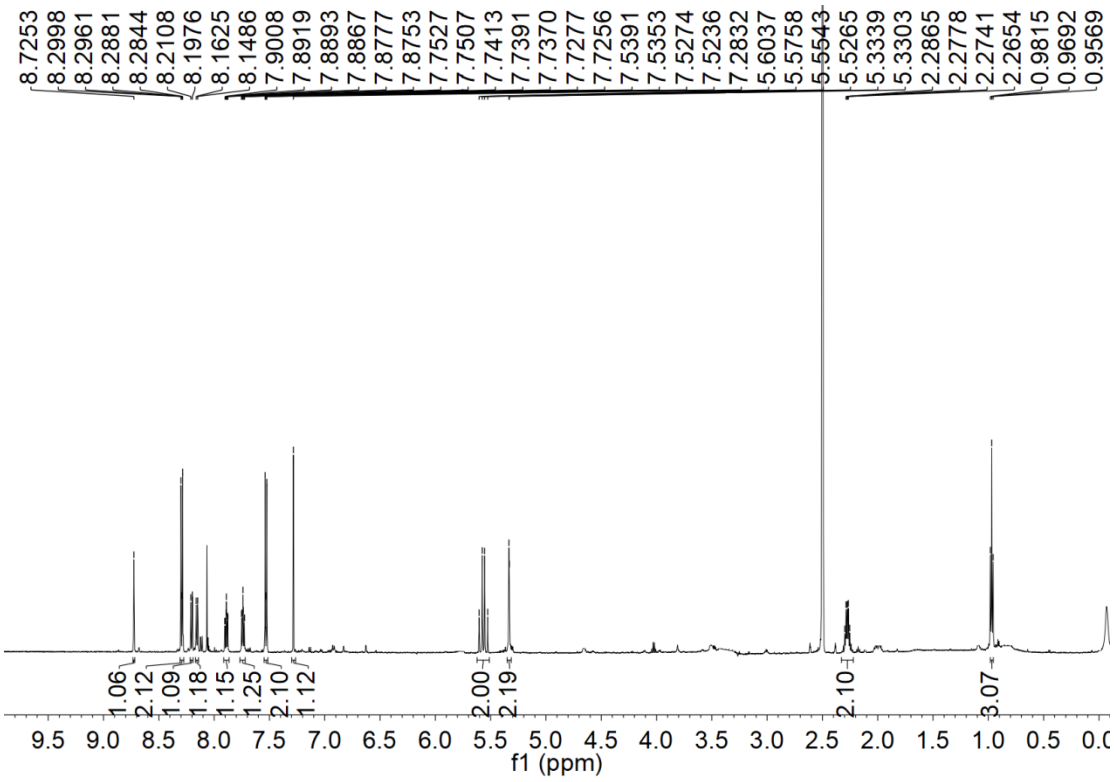


**D**

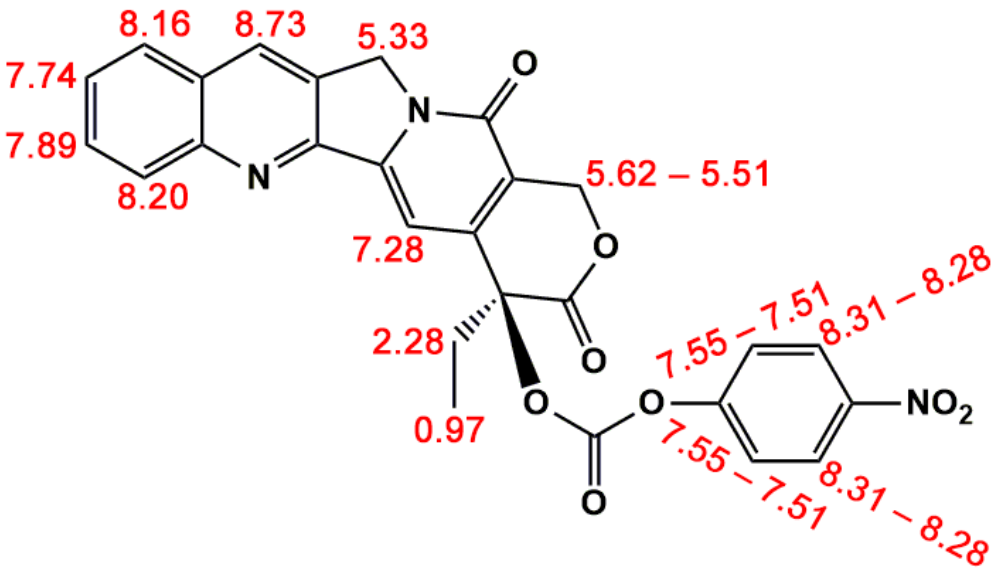


**Figure S2** 1H NMR spectra of (A) PPA-DA, and (C) N-CPT, chemical shift of (B) PPA-DA, and (D) N-CPT.

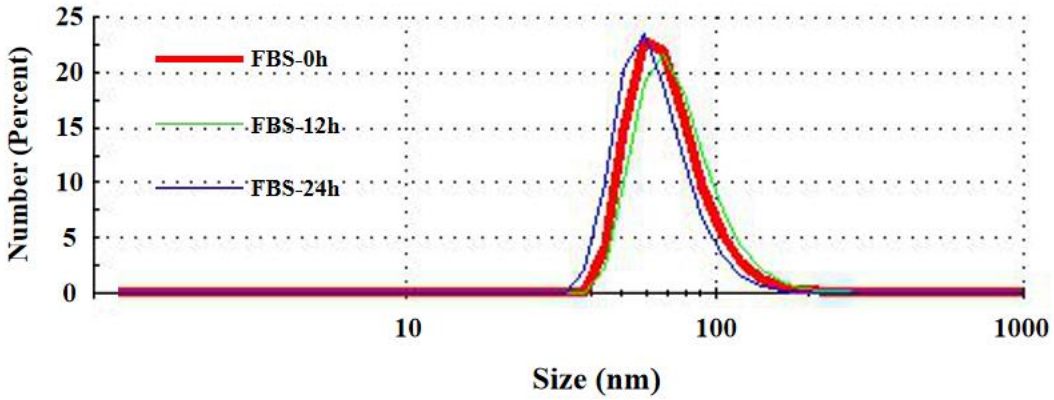


**Figure S3** DLS size profiles of co-nanoassemblies incubated with various times (0, 12 and 24 h) under the simulated *in vivo* environment.

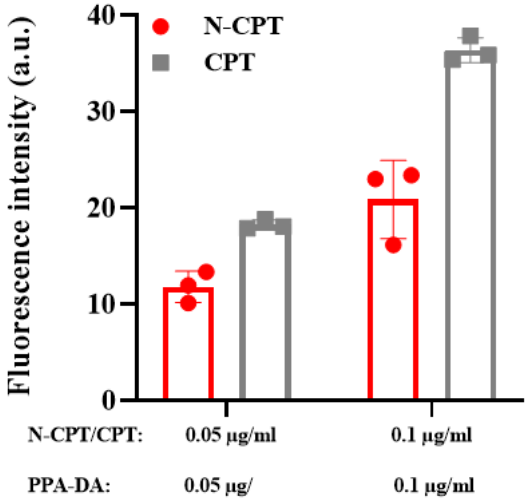


**Figure S4** Fluorescence intensity of PPA-DA&N-CPT complex and PPA-DA&CPT complex under various concentrations.

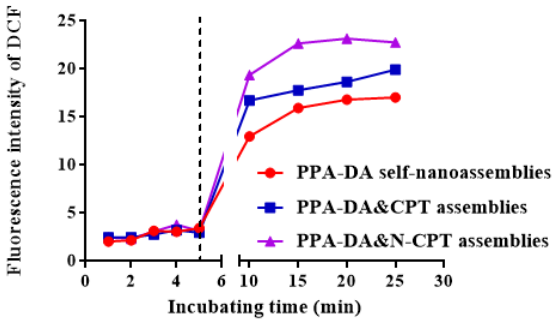


**Figure S5** Generation of singlet oxygen by increased fluorescence intensity of DCFH-DA in the absence of PPA-DA self-nanoassembly, PPA-DA & CPT co-nanoassemblies, and PPA-DA & N-CPT co-nanoassemblies within tumor cells (660 nm, 20 mW/cm$^2$).

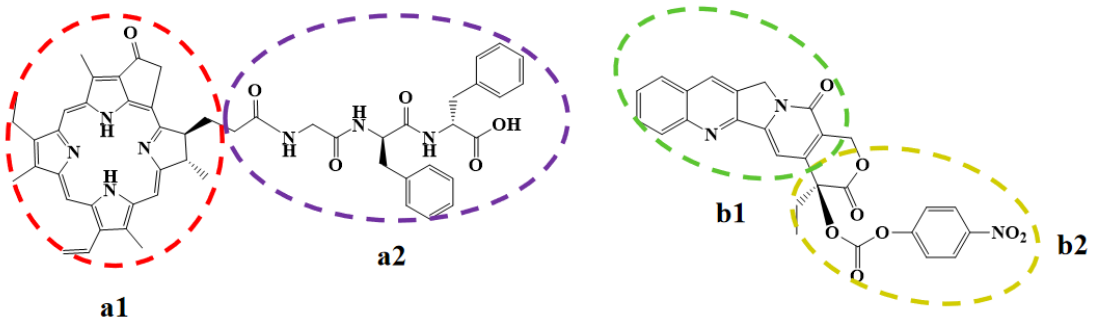


**Figure S6** Schematic illustration of the coarse-graining scheme for the co-nanoassembly system: the bead model of PPA-DA for which two beads “a” were defined to constitute one single pheophorbide a-diphenylalanine peptide molecule, one single N-CPT molecule was designated to represent two beads “b”.

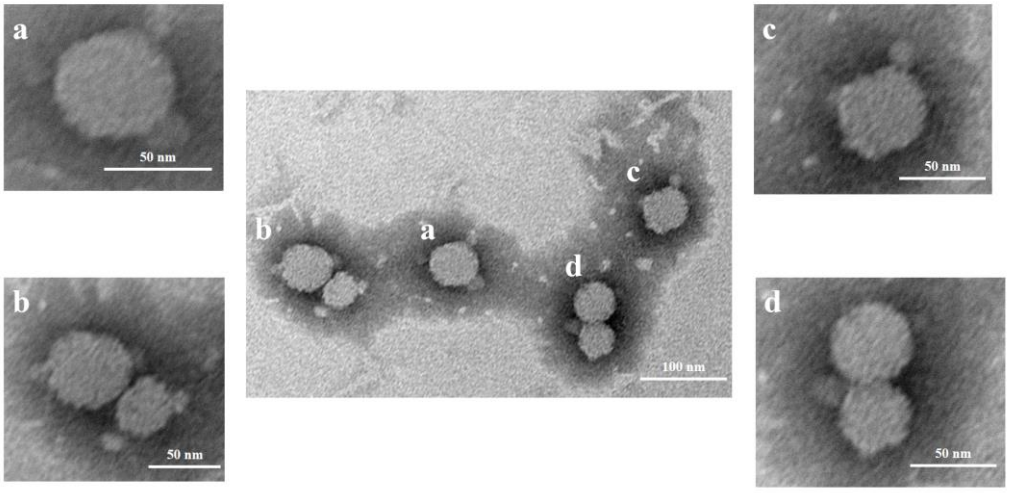


**Figure S7** TEM images of non-PEGylated co-nanoassemblies.

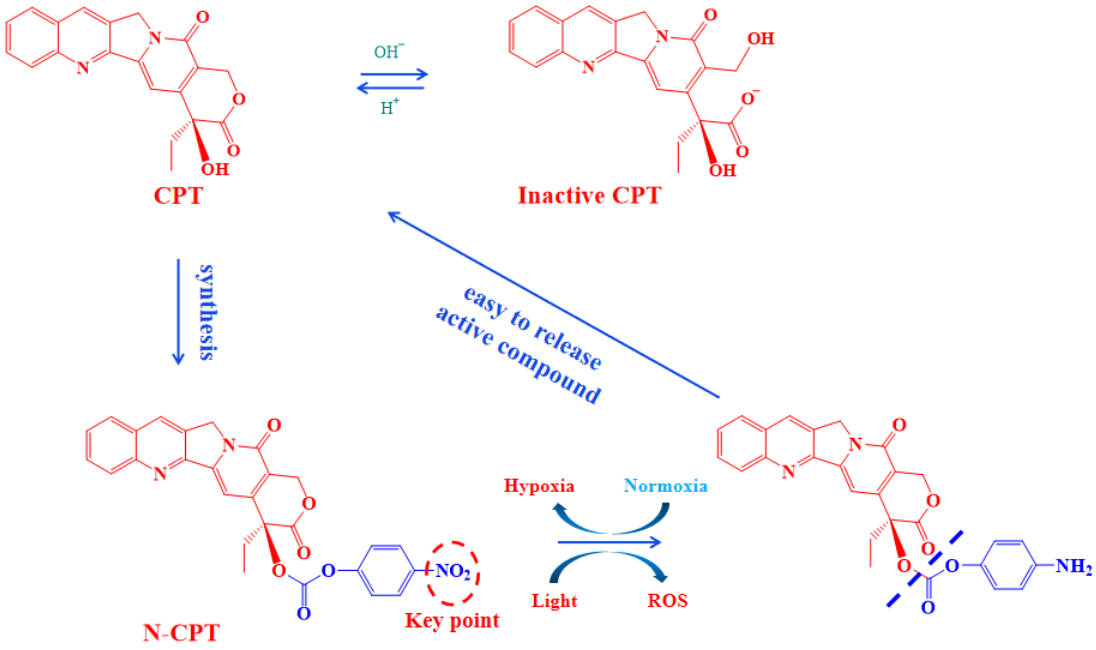


**Scheme S2** Proposed mechanism of hypoxia-mediated activation of CPT prodrug and inactivation of CPT.

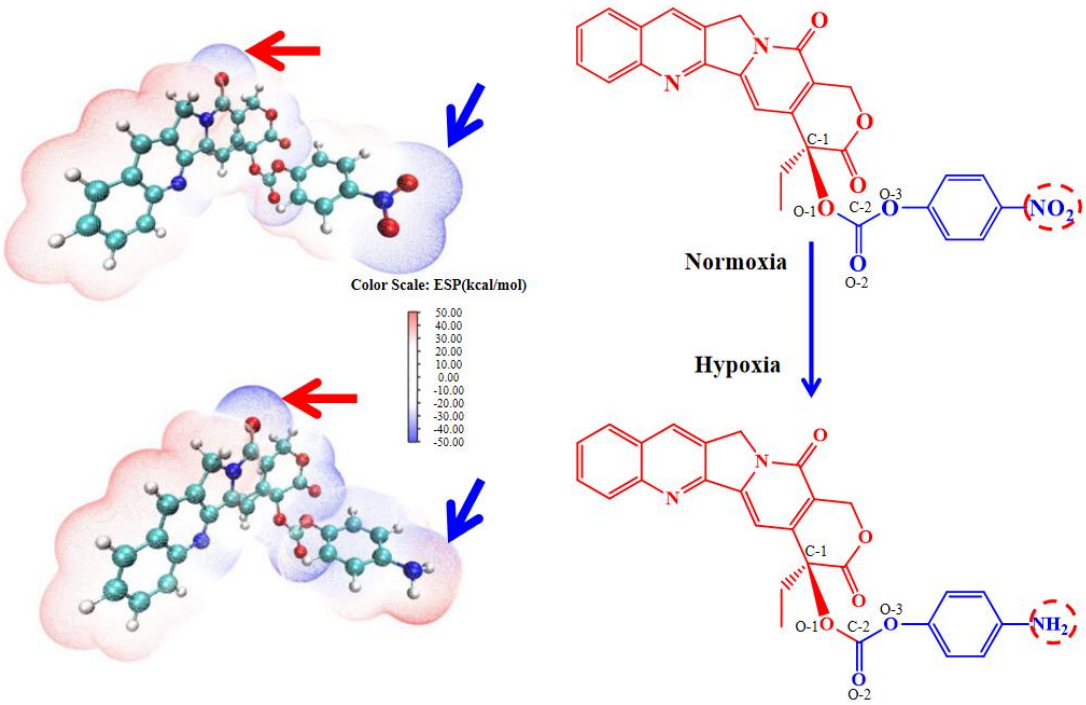


**Figure S8** The visual plots of electrostatic potential and chemical structures of N-CPT and reduced N-CPT. Red means positive potential and blue is negative potential.

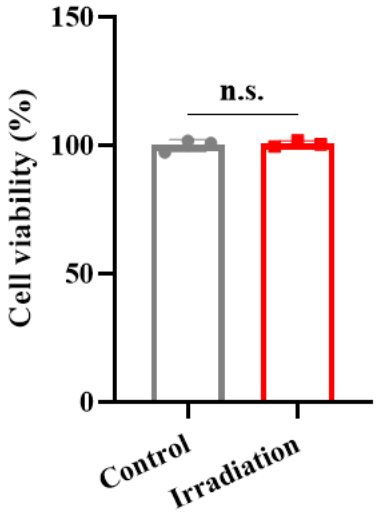


**Figure S9** Cytotoxicity of co-nanoassemblies-free incubated with 24 h after 660 nm laser irradiation (20 mW/cm$^2$) for 3 min ($n$=3).

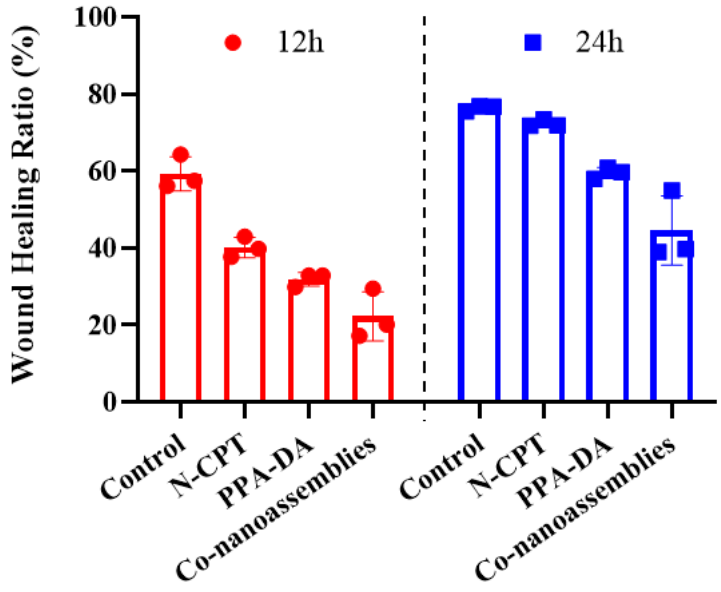


**Figure S10** Quantitation of 4T1 cells wound healing at various time (12 and 24 h) was presented.

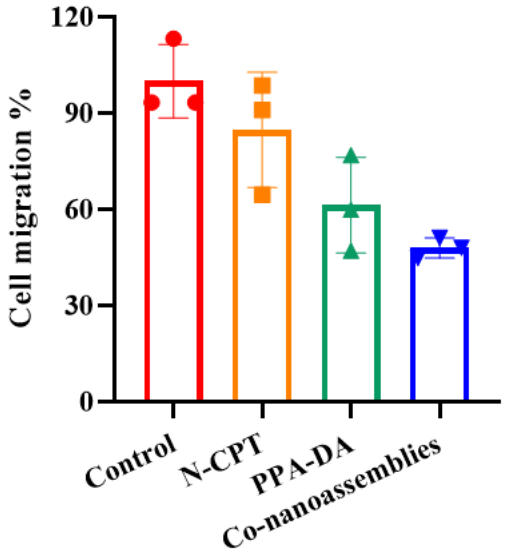


**Figure S11** 4T1 cells representative quantitation images of migration assays at 24 h.

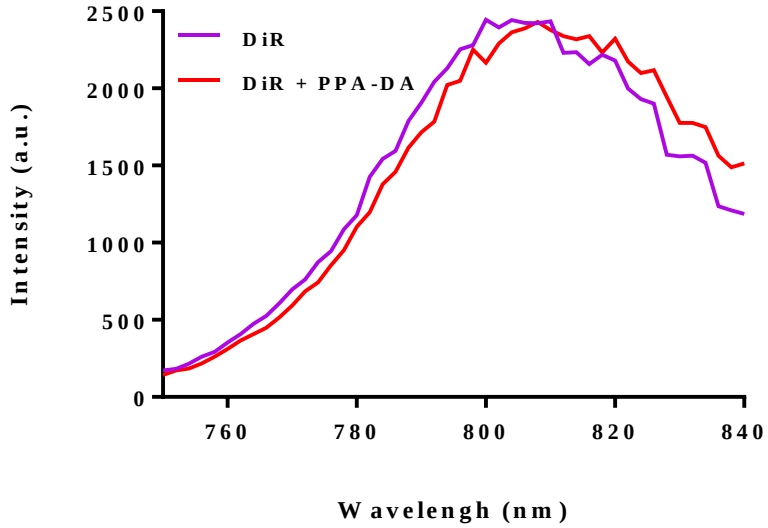


**Figure S12** Fluorescence spectra of DiR and a mixture of DiR and PPA-DA.

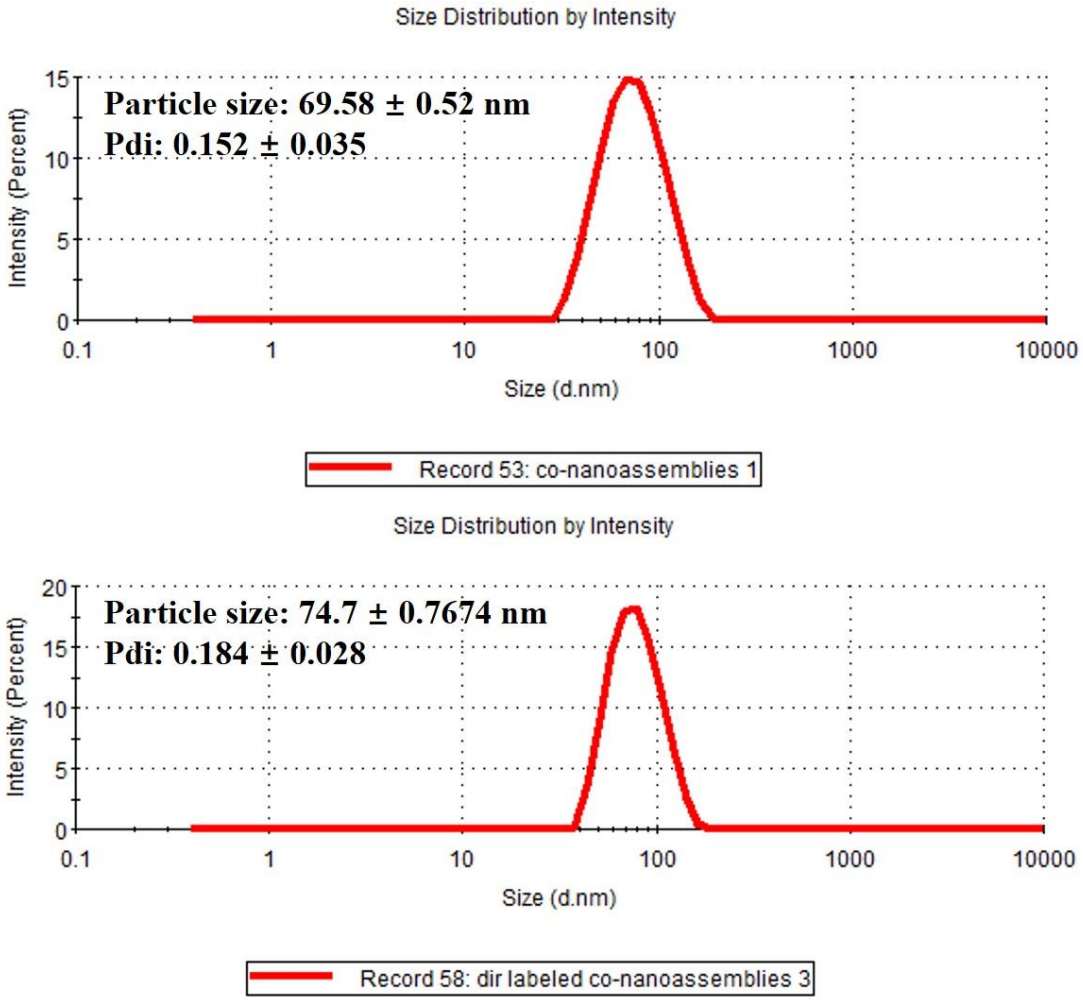


**Figure S13** Dynamic light scattering (DLS) profile of top: co-nanoassemblies, bottom: DiR labeled co-nanoassemblies.

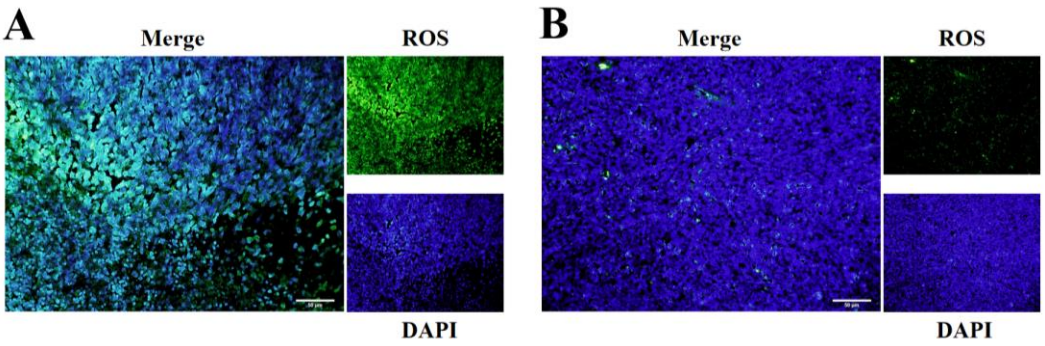


**Figure S14** Inverted fluorescence microscope images of laser-induced intratumoral ROS. generation of co-nanoassemblies with (A)/without (B) the laser irradiation treated 4T1tumor-bearing Balb/c mice *in vivo*.

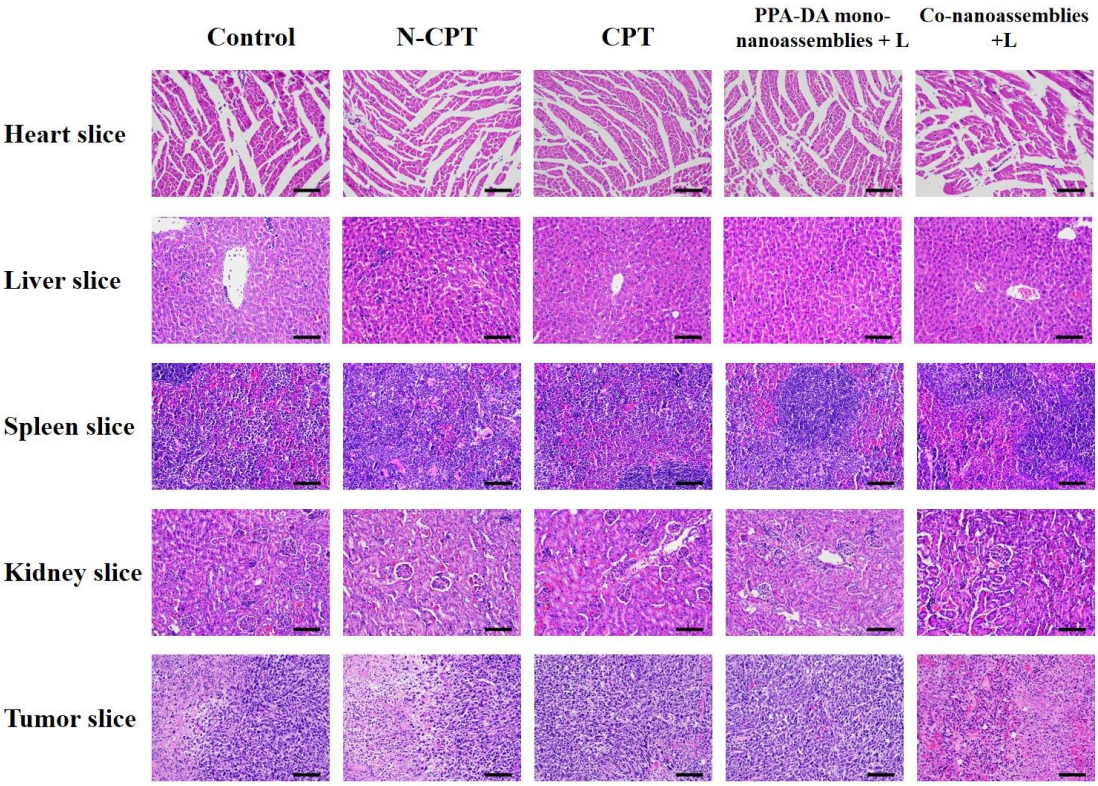


**Figure S15** H&E staining images in organs after the treatment with control, N-CPT, CPT, PPA-DA mono-nanoassemblies+L, and co-nanoassemblies+L on the mouse 4T1 orthotopic breast cancer model, scale bar represents 100 μm.

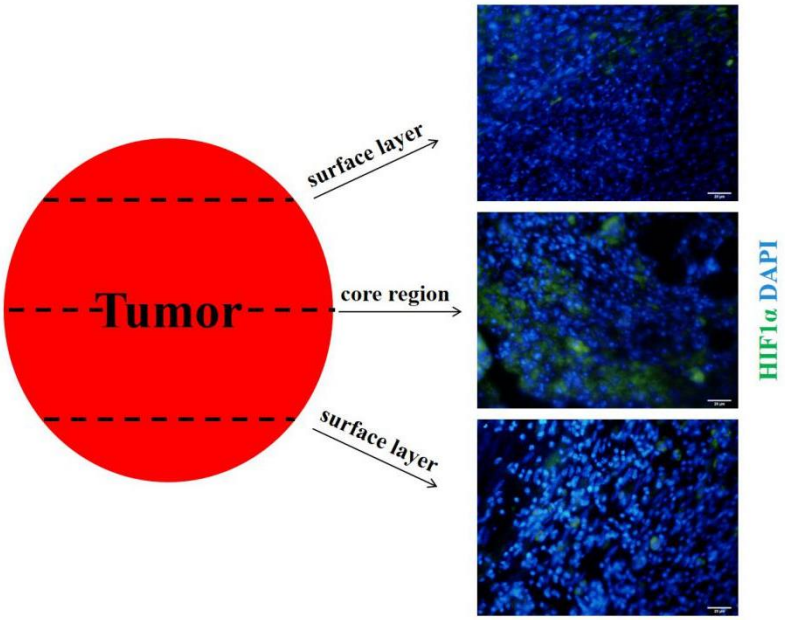


**Figure S16** Transverse sections of untreated tumor (Scale bar: 20 μm).

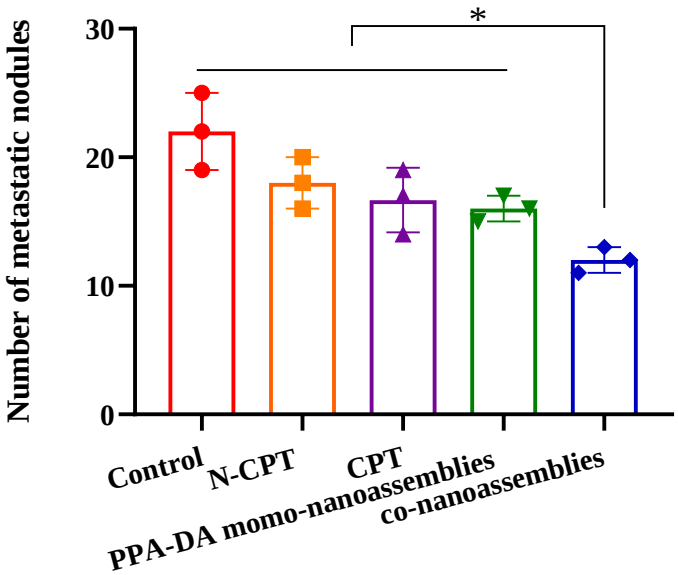


**Figure S17** Therapeutic protocol on mouse 4T1 subcutaneous tumor xenograft. Number quantities of the lung metastases under the treatment. Data presented are the means ± SD, **P*<0.05, ***P* < 0.01 and ****P* < 0.001 by two-tailed student's *t* test.

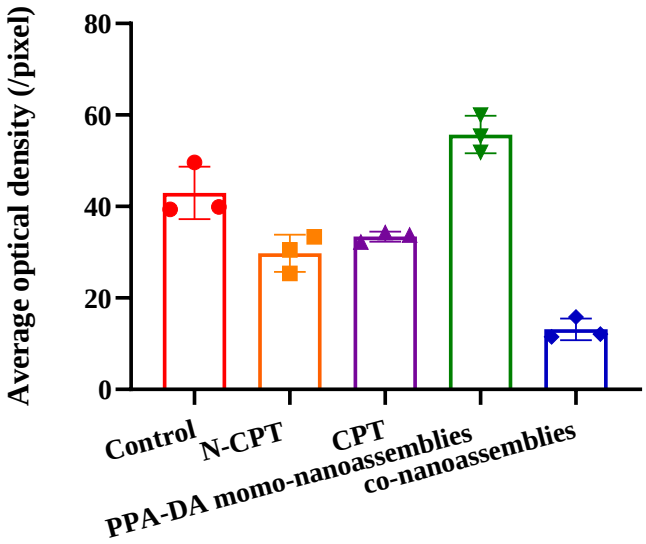


**Figure S18** Therapeutic protocol on mouse 4T1 subcutaneous tumor xenograft. Average fluorescent density of HIF1$\alpha$ tumor accumulation was presented. Data presented are the means ± SD.

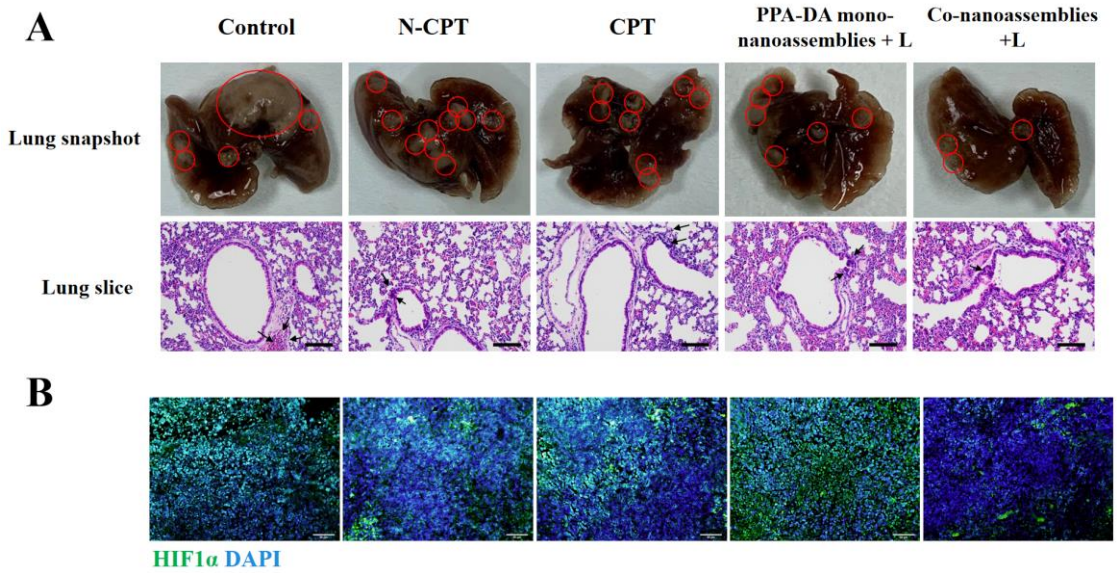


**Figure S19** Photos of whole lungs and H&E staining of the lung slices collected from different groups of mice after various treatments on the mouse 4T1 orthotopic breast cancer model, scale bar represents 100 μm.

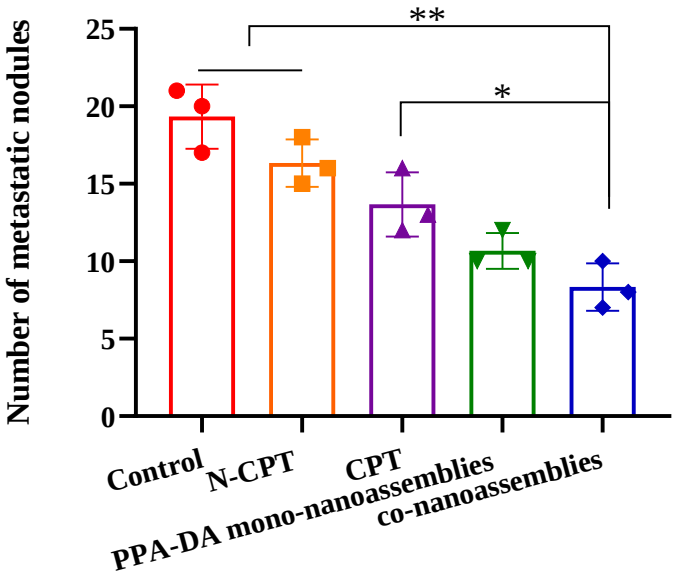


**Figure S20** Therapeutic protocol on mouse 4T1 orthotopic tumor xenograft. Number quantities of the lung metastases under the treatment. Data presented are the means ± SD, *$P$ < 0.05, **$P$ < 0.01 and ***$P$ < 0.001 by two-tailed student's $t$ test.

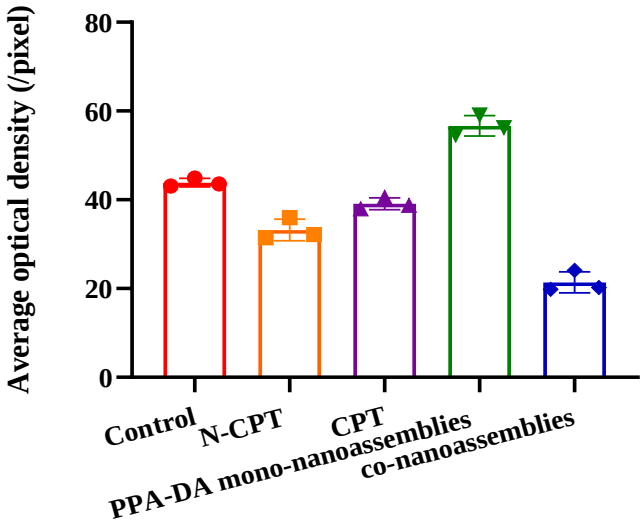


**Figure S21** Therapeutic protocol on mouse 4T1 orthotopic tumor xenograft. Average fluorescent density of HIF1$\alpha$ tumor accumulation was presented. Data presented are the means ± SD.

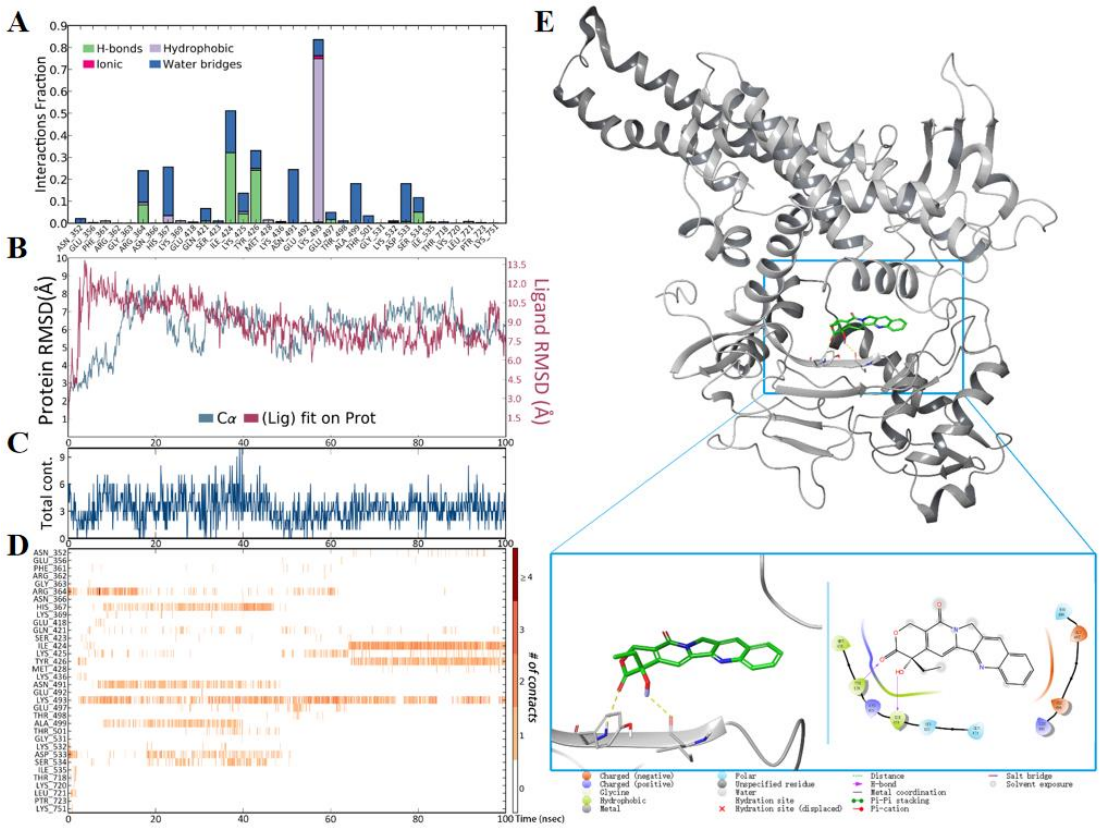


**Figure S22** Molecular dynamics statistical results of topoisomerase I (PDB ID: 1K4D) with CPT and their interaction features. (A) Interaction bar chart of ligand and residues around binding site. (B) RMSD line chart of topoisomerase I (red) and camptothecin (blue). (C) Total interactions number of the complex along the simulation time. (D) Interaction timeline chart of residues around the binding site. (E) 3D and 2D interactions of the complex. Protein was in grey ribbon and the ligand was in green.

**Table S1** Diameter distribution of PEGylated mono-nanoassembly PPA-DA (the weight ratio of drug to PEG).

| | PPA-DA | PPA-DA +5% PEG | PPA-DA +10% PEG | PPA-DA +15% PEG | PPA +15% PEG | 15% PEG |
|---|---|---|---|---|---|---|
| **Size (nm)** | 40.72±5.018 | 66.21±2.480 | 62.16±0.5658 | 63.43±1.373 | -- | -- |
| **PDI** | 0.374±0.045 | 0.218±0.047 | 0.199±0.019 | 0.163±0.040 | -- | -- |

**Table S2** The docking energies (kcal/mol) *via* two molecular docking softwares.

| | PPA-DA & N-CPT | PPA-DA & CPT |
|---|---|---|
| **Autodock** | –6.9 | –6.8 |
| **Vina** | –7.38 | –6.49 |

**Table S3** The pharmacokinetics parameters.

| | $AUC_{0-t}$ (μg/ml*h) | $C_{max}$ (μg/ml) | $T_{1/2}$ (h) |
|---|---|---|---|
| **N-CPT from co-nanoassembly** | 2611.55±244.38 | 452.14±125.77 | 13.91±4.20 |
| **Free N-CPT** | 222.61±28.24 | 48.04±7.72 | 13.93±13.19 |

**Table S4** Solubility Parameter.

| | Bead | Solubility parameter |
|---|---|---|
| PPA-DA | a1 | 14.5 |
| | a2 | 24.5 |
| N-CPT | b1 | 24.7 |
| | b2 | 21.8 |
| Water | w | 46 |

**Table S5** The interaction parameters ($a_{ij}$) in DPD simulation (DPD-reduced unit: $k_{BT}/r_c$).

| | *w* | *a*1 | *a*2 | *b*1 | *b*2 |
|---|---|---|---|---|---|
| *w* | 78 | | | | |
| *a*1 | 148.7 | 78 | | | |
| *a*2 | 111 | 85.1 | 78 | | |
| *b*1 | 110.3 | 85.4 | 78 | 78 | |
| *b*2 | 119.8 | 81.8 | 78.5 | 78.6 | 78 |